

The mass of charged pions in neutron star matter

Bryce Fore,¹ Norbert Kaiser,² Sanjay Reddy,¹ and Neill C. Warrington¹

¹*Institute for Nuclear Theory and Department of Physics, University of Washington, Seattle, WA 98195.*

²*Physik-Department T39, Technische Universität München, D-85747 Garching, Germany*

(Dated: January 19, 2023)

We examine the behavior of charged pions in neutron-rich matter using heavy-baryon chiral perturbation theory. This study is motivated by the prospect that pions, or pion-like, excitations, may be relevant in neutron-rich matter encountered in core-collapse supernovae and neutron star mergers. We find, as previously expected, that the π^- mass increases with density and precludes s-wave condensation, and the mass of the π^+ mode decreases with increasing density. The energy difference between neutrons and protons in neutron-rich matter related to the nuclear symmetry energy alters the power counting. It enhances higher-order contributions to the pion self-energy. Previously unimportant but attractive diagrams are now enhanced. The net effect of this is the appearance of a new collective mode with the quantum numbers of the π^+ , and a pronounced reduction of the π^+ mass.

I. INTRODUCTION

The study of pions in dense nuclear matter has a long and storied history. In a pioneering work in the 1970s, Sawyer and Scalapino proposed that pion condensation might lower the energy of nuclear matter at high density [1–3]. In subsequent years, several authors studied its manifestation and implications for nuclei and neutron stars in some detail using simple models for the pion-nucleon interaction [4–11]. Pion condensation occurs at low temperatures when the energy to produce a pion is less than its associated chemical potential. Earlier work has addressed the possibility of condensation of negatively charged pions in neutron stars because the chemical potential for negative charge, which we denote throughout as $\hat{\mu}$, increases with density and is typically in the range 100–300 MeV in the neutron star core. In the absence of interactions, a pion condensate with zero-momentum will occur when $\hat{\mu} \geq m_\pi$, where $m_\pi \simeq 140$ MeV is the mass of the pion. However, repulsive s-wave interactions between π^- and neutrons increased the pion energy in neutron stars and were believed to disfavor condensation of zero-momentum pions.

In contrast, a strongly attractive p-wave interaction between pions and nucleons was shown to favor condensation of pions with momentum $k_\pi \simeq m_\pi$ and lead to a non-uniform ground state [7]. In the 1980s, more sophisticated but model-dependent analyses, including many-body corrections and correlations between nucleons at short distances, found that even p-wave condensation may not be robust at the densities encountered in neutron stars (for a comprehensive review see [12]). Consequently, the interest in pion condensation has waned over the years.

In this paper, we revisit the calculation of the energy of zero-momentum charged pions in dense neutron-rich matter using heavy-baryon chiral perturbation theory ($\text{HB}\chi\text{PT}$) at two-loop order. We do so for the following reasons. First, earlier calculations of the energy shift due to the nuclear medium were computed in the mean-field approximation and based on simple models for the pion-nucleon interaction, which were poorly constrained by pion-nucleon scattering data. Second, earlier calculations also neglected the effect of the nuclear symmetry energy, which induces a large energy difference between neutrons and protons in neutron-rich matter. Finally, even in the absence of pion condensation, the mass of pionic excitations in the medium is relevant to the description of the ground state and response properties of dense nuclear matter at finite temperatures realized in extreme astrophysical phenomena such as neutron star mergers and core-collapse supernovae [13].

We present results for all two-loop diagrams that contribute to the pion self-energy in dense neutron-rich matter using heavy-baryon chiral perturbation theory ($\text{HB}\chi\text{PT}$) and augment these diagrams with two pieces of modeling. First, we incorporate a model of the nucleon self-energy into all nucleon lines. This nucleon self-energy incorporates energy shifts of the neutrons & protons in the dense nuclear medium. We additionally replace bare $\pi N \rightarrow \pi N$ vertices with their full T-matrix counterparts to account for the energy dependence of the pion self-energy. Such T-matrix modifications have proven crucial in understanding the binding energies of pionic atoms [14, 15]. We find that previously-neglected two-loop diagrams (involving p-wave interactions in the intermediate state) and the inclusion of in-medium nucleon self-energies lower the pion self-energy relative to previous estimates. In particular, small energy denominators in perturbation theory are produced when the energy difference between neutrons and protons becomes of the order of the pion mass. These small energy denominators promote the importance of certain attractive Feynman diagrams, which lower the π^- energy; this modified power counting is one of the central findings of this work. Modified power counting is further supported by a recent analysis of experimental data suggesting that the nuclear symmetry energy - the in-medium energy difference between protons and neutrons - can be large at densities of interest to neutron stars. Finally, we find a collective mode with the quantum numbers of the π^+ in the medium.

The calculation presented here improves upon the systematic calculations of the pion self-energy in asymmetric matter using χPT presented in Refs. [14, 15]. We include all diagrams considered by previous authors while including several others. Interestingly, we find that the self-energy for a pion at rest is insensitive to the short-distance, repulsive, spin-isospin correlations between nucleons that are known to play a key role in inhibiting p-wave condensation [9]. This feature, again, lowers the π^- self-energy relative to previous estimates.

The material in this paper is organized as follows. In Section II, we describe our two-loop $\text{HB}\chi\text{PT}$ calculation of the pion self-energy in isospin-asymmetric dense matter. In Section III, we present a parametric model to account for strong interactions between nucleons and study its effect on the pion self-energy. Finally, in Section V, we summarize our findings and discuss their limitations.

II. PION SELF-ENERGY IN NEUTRON-RICH MATTER FROM $\text{HB}\chi\text{PT}$

The dispersion relation of the pion and pion-like collective excitations in dense neutron-rich matter is obtained from the poles of the in-medium pion propagator. Employing $\phi(x)$ as the field operator that destroys a π^- particle, we

adopt the standard definition for the propagator:

$$iD(\omega, k) = \int d^4x \langle T\phi(x)\phi^\dagger(0) \rangle e^{i(\omega x_0 - \vec{k}\cdot\vec{x})} = \frac{i}{\omega^2 - k^2 - m_\pi^2 - \Pi(\omega, k)}, \quad (1)$$

with $k = |\vec{k}|$. The quantity $\Pi(\omega, k)$ is the pion self-energy in nuclear matter and depends implicitly on the baryon and isospin densities. The dispersion relations for both the π^- and π^+ , as well as that of pion-like collective modes, can be obtained as solutions of the equation

$$\omega^2 - k^2 - m_\pi^2 - \Pi(\omega, k) = 0, \quad (2)$$

where ω and k are the pion energy and momentum. The sign of the residue at the pole determines the particle's charge corresponding to a given pole [12].

In this study, we will consider the dispersion relation of a pion at rest in the medium, denoting $\Pi(\omega, 0) = \Pi(\omega)$. This restriction comes from our initial motivation of exploring s-wave pion condensation in neutron stars; however, as we will see later on, we find no evidence for this. Nevertheless, $\Pi(\omega)$ gives access to long-wavelength properties of pion-like excitations in dense matter. To calculate $\Pi(\omega)$, we will need a description of pion-nucleon, pion-pion, and nucleon-nucleon interactions, choosing HB χ PT as a systematic framework to accomplish this. This effective field theory organizes all interactions consistent with chiral symmetry in a derivative expansion and is expected to be reliable when the pion and nucleon momenta are much smaller than $\Lambda \simeq 4\pi f_\pi \simeq 1$ GeV, where $f_\pi = 92.2$ MeV is the pion decay constant.

The energy and momentum scales relevant to our calculation are set by the pion energy $\omega = \hat{\mu} \simeq m_\pi$, and the nucleon Fermi momentum $k_F = (3\pi^2 n_B/2)^{1/3} \simeq 263$ MeV $(n_B/n_{\text{sat}})^{1/3}$, with $n_{\text{sat}} \simeq 0.16$ fm $^{-3}$ the saturation density. In what follows, we calculate $\Pi(\omega)$ by retaining terms up to order k_F^5 and $\omega_{\pi^-}^2$. For this purpose, it is adequate to work with the following heavy-baryon Lagrangian [16, 17]

$$\mathcal{L}_{\pi\pi}^{(2)} + \mathcal{L}_{\pi N}^{(1)} + \mathcal{L}_{\pi N}^{(2)} + \mathcal{L}_{\pi NN}^{(1)}, \quad (3)$$

where the superscript denotes the chiral dimension, i.e., the number of derivatives and/or insertions of the pion mass. Interactions between pions at leading order are given by

$$\mathcal{L}_{\pi\pi}^{(2)} = \frac{f_\pi^2}{4} \text{tr}(\partial_\mu U \partial^\mu U^\dagger + \chi_+), \quad (4)$$

with the pion fields (π^+, π^0, π^-) contained in the special unitary 2×2 matrix

$$U = \exp\left(\frac{i}{f_\pi} \begin{bmatrix} \pi^0 & \sqrt{2}\pi^+ \\ \sqrt{2}\pi^- & -\pi^0 \end{bmatrix}\right),$$

and the term $\chi_+ = m_\pi^2(U + U^\dagger)$ introduces explicit chiral symmetry breaking. Interaction terms between pions and nucleons in leading order are given by

$$\mathcal{L}_{\pi N}^{(1)} = \bar{N}(iv \cdot D + g_A S \cdot u)N, \quad (5)$$

where $v_\mu = (1, \vec{0})$ is the four-velocity and $S^\mu = (0, \vec{\sigma}/2)$ the spin-vector of the nucleon. Furthermore, $g_A = 1.27$ denotes the axial-vector coupling constant. The chiral covariant derivative and axial-vector quantity are defined as $D_\mu = \partial_\mu + \frac{1}{2}[\xi^\dagger, \partial_\mu \xi]$ and $u_\mu = i(\xi^\dagger \partial_\mu \xi - \xi \partial_\mu \xi^\dagger)$, with $\xi = \sqrt{U}$.

Seven terms contribute to the Lagrangian at next-to-leading order (NLO) [16]; however, we display here only those operators that contribute to the self-energy of a zero-momentum pion. This part of the chiral πN Lagrangian reads

$$\mathcal{L}_{\pi N}^{(2)} = \bar{N} \left(-\frac{ig_A}{2M} \{S \cdot D, v \cdot u\} + c_1 \text{tr} \chi_+ + \left(c_2 - \frac{g_A^2}{8M}\right) (v \cdot u)^2 + c_3 u \cdot u \right) N, \quad (6)$$

where the first term is a relativistic $1/M$ -correction to the pion-nucleon vertex, and c_1, c_2, c_3 are low-energy constants (LEC's). Pions also couple to a two-nucleon axial current at NLO and this interaction is described by

$$\mathcal{L}_{\pi NN}^{(1)} = \frac{c_D}{2f_\pi^2 \Lambda_\chi} (\bar{N}N)(\bar{N}S \cdot uN). \quad (7)$$

with the scale $\Lambda_\chi \simeq 700$ MeV and c_D a dimensionless parameter. The interaction in Eq.(7) generates a one-pion exchange three-nucleon force, and therefore c_D has been determined from the triton binding energy and the neutron-deuteron doublet scattering length [18]. Its value is sensitive to the regularization scheme and choice of cutoff in the

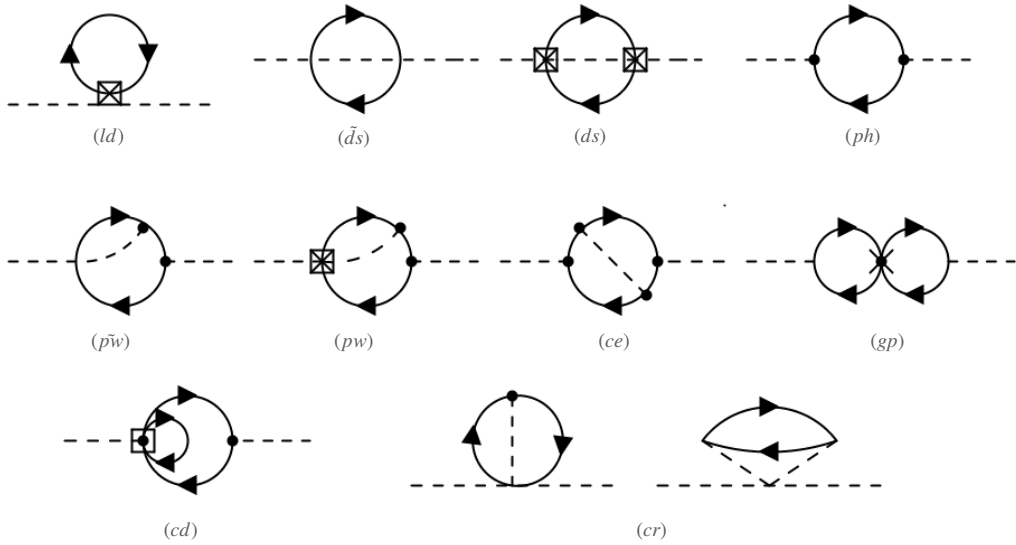


FIG. 1: Feynman diagrams contributing to the pion self-energy. Solid and dashed lines represent nucleons and pions, respectively. There are several types of vertices: the Weinberg-Tomozawa 2π -vertex is undecorated, the dot represents the axial pion-nucleon vertex, the hatched-box represents T-matrix insertions, the open-box is the pion coupling to four nucleons, and the cross-dot indicates a short-distance nucleon-nucleon interaction.

chiral two-nucleon potential. For momentum-space cutoffs between 500 MeV and 600 MeV, c_D falls into the range $-4 < c_D < 1$ [18].

The Feynman diagrams contributing to the pion self-energy at two-loop order are shown in Fig. 1. Some time ago the contributions due to the diagrams labelled (ld), ($\tilde{d}s$), (ph), and (cr) have been calculated in Refs.[14, 15]. The diagram labeled (ld) includes contributions linear in the proton and neutron density and is given by

$$\Pi_{ld}(\omega) = T^-(\omega) \frac{k_n^3 - k_p^3}{3\pi^2} - T^+(\omega) \frac{k_n^3 + k_p^3}{3\pi^2}, \quad (8)$$

where k_n and k_p denote the neutron and proton Fermi momenta, and $T^\mp(\omega)$ are the isospin-odd and isospin-even s-wave off-shell πN scattering amplitudes. The isospin-odd amplitude (restricted to its real part) is given up to order ω^3 by:

$$T^-(\omega) = \frac{\omega}{2f_\pi^2} + \frac{\gamma\omega^3}{8\pi^2 f_\pi^4} - \frac{\omega^2 Q}{8\pi^2 f_\pi^4} \ln \frac{\omega + Q}{m_\pi}, \quad (9)$$

where $Q = \sqrt{\omega^2 - m_\pi^2}$ and γ is chosen such that the empirical value $T^-(m_\pi) = 1.85$ fm is obtained. The leading term of T^- , first predicted by Weinberg and Tomozawa [19, 20], is remarkably close to the empirical value, and chiral perturbation theory converges well for this quantity. In contrast, the convergence of $T^+(\omega)$ is known to be poor. Up to order ω^3 , its real part is given by

$$T^+(\omega) = \frac{\sigma_N - \beta\omega^2}{f_\pi^2} + \frac{3g_A^2 m_\pi^3}{16\pi f_\pi^4} + \frac{3g_A^2 m_\pi Q^2 \zeta}{64\pi f_\pi^4}, \quad (10)$$

where $\sigma_N = -4c_1 m_\pi^2 - 9g_A^2 m_\pi^3 / 64\pi f_\pi^2$ is the pion-nucleon sigma term [21] and $\beta = -2(c_2 + c_3) + g_A^2 / 4M$. In Ref. [14] the low-energy constant c_1 is chosen to reproduce $\sigma_N \simeq 45 \pm 15$ MeV, the range probed by phenomenological and lattice calculations [22, 23], and the combination $c_2 + c_3$ is determined by the empirical value $T^+(m_\pi) \simeq 0$. The off-shell parameter ζ encodes the freedom of choosing the interpolating pion field. Its value is scheme-dependent and needs to be estimated by fits to data. In Ref. [14], the authors set $\zeta = 0$ to ensure that the residue at the pole of the pion propagator in the vacuum is one. However, this choice introduces systematic uncertainties because the convergence of the χ PT expansion for $T^+(\omega)$ is not well-understood. To incorporate this uncertainty, and assuming that $Q^2 \ll m_\pi^2$, we rewrite the scattering amplitude as

$$\tilde{T}^+(\omega) = -\frac{\tilde{\sigma}}{f_\pi^2} \frac{Q^2}{m_\pi^2}, \quad (11)$$

where $\tilde{\sigma} \simeq \sigma_N$ is treated as model parameter with values in the range $40 \dots 80$ MeV. Later, we will use constraints on the π^- optical potential in ^{208}Pb to justify this choice.

The contribution to $\Pi(\omega)$ from the two-loop diagram labeled \tilde{ds} accounts for double-scattering due to the Weinberg-Tomozawa interaction and is given by

$$\Pi_{\tilde{ds}} = \frac{\omega^2}{3(4\pi f_\pi)^4} \left\{ L(\omega; k_n, k_n) + L(\omega; k_p, k_p) + 2L(\omega; k_n, k_p) \right\}, \quad (12)$$

with the logarithmic function

$$\begin{aligned} L(\omega; k_n, k_p) = & 4k_n k_p (3k_n^2 + 3k_p^2 + Q^2) + 8Q(k_n^3 - k_p^3) \ln \frac{Q + k_n - k_p}{|Q - k_n + k_p|} - 8Q(k_n^3 + k_p^3) \ln \frac{Q + k_n + k_p}{|Q - k_n - k_p|} \\ & + \left[3(k_n^2 - k_p^2)^2 + 6Q^2(k_n^2 + k_p^2) - Q^4 \right] \ln \frac{|(k_n - k_p)^2 - Q^2|}{|(k_n + k_p)^2 - Q^2|}, \end{aligned} \quad (13)$$

with $Q = \sqrt{\omega^2 - m_\pi^2}$ for $\omega > m_\pi$. The diagram labeled (ds) includes higher-order contributions to double-scattering. This contains contributions up to order ω^3 that were included in the off-shell scattering amplitudes $T^\pm(\omega)$ defined earlier. Including these contributions, we find

$$\Pi_{ds} = \frac{1}{192\pi^4} \left\{ T_{nn}(\omega)^2 L(\omega; k_n, k_n) + T_{pp}(\omega)^2 L(\omega; k_p, k_p) + T_{np}(\omega)^2 L(\omega; k_n, k_p) \right\}, \quad (14)$$

where $T_{nn}(\omega) = T^+(\omega) - T^-(\omega)$, $T_{pp}(\omega) = T^+(\omega) + T^-(\omega)$, and $T_{np}(\omega) = -\sqrt{2}T^-(\omega)$.

The particle-hole diagram (labeled (ph) in Fig. 1) contains the contribution due to the pseudovector interaction between nucleons and pions. Since the pion momentum is zero, this contribution appears first as relativistic correction suppressed by the factor $(k_{p,n}/M)^2$, and is given by

$$\Pi_{ph}(\omega) = \frac{g_A^2 \omega}{f_\pi^2} \left(\frac{k_p^5 - k_n^5}{10\pi^2 M^2} \right). \quad (15)$$

We note that the particle-hole contribution is also suppressed in systems with small isospin asymmetries. For these reasons, the attractive contribution from Π_{ph} is relatively unimportant in the analysis of pionic atoms [14]. However, we shall find that this diagram contributes to the pion self-energy in neutron stars.

The two-loop diagram labeled (pw) includes the attractive p-wave pion-nucleon interaction in the intermediate state. In Fig. 1 we only show one of several possible intermediate states. Others are obtained by connecting the p-wave vertex to the lower Fermion line and by switching the location of the Weinberg-Tomazawa vertex. The intermediate pion can be either a neutral pion or charged pion. We have calculated the contribution from all of these diagrams, and their sum is given by

$$\Pi_{\tilde{pw}}(\omega) = \frac{g_A^2 \omega}{4Mf_\pi^4} \left\{ 2I(\omega; k_p, k_p) - 2I(\omega; k_n, k_n) - 2K(\omega; k_n, k_p) + I(0; k_p, k_p) - I(0; k_n, k_n) - K(0; k_n, k_p) \right\}, \quad (16)$$

where the sum originates from all possible arrangements of the Weinberg-Tomozawa (WT) and dotted vertices. The functions $I(\omega; k_n, k_p)$ and $K(\omega; k_n, k_p)$ arise from the following principal-value integrals of a pion propagator over two Fermi spheres:

$$\begin{aligned} I(\omega; k_n, k_p) &= \int \frac{d^3 l_1 d^3 l_2}{(2\pi)^6} \theta(k_n - |\vec{l}_1|) \theta(k_p - |\vec{l}_2|) \frac{(\vec{l}_1 - \vec{l}_2)^2}{(\vec{l}_1 - \vec{l}_2)^2 + m_\pi^2 - \omega^2}, \\ K(\omega; k_n, k_p) &= \int \frac{d^3 l_1 d^3 l_2}{(2\pi)^6} \theta(k_n - |\vec{l}_1|) \theta(k_p - |\vec{l}_2|) \frac{2(\vec{l}_1^2 - \vec{l}_2^2)}{(\vec{l}_1 - \vec{l}_2)^2 + m_\pi^2 - \omega^2}. \end{aligned} \quad (17)$$

We provide explicit analytical expressions for these functions in the appendix.

It is straightforward to include higher-order terms in ω contributing to the (pw) diagram. The net effect of inserting further pion-nucleon vertices is to replace the WT vertex with the off-shell amplitudes, as was obtained in Eq. 14 for the double-scattering contribution. This also allows for the incorporation of the isospin-even contributions, and we find

$$\begin{aligned} \Pi_{pw}(\omega) &= T^-(\omega) \frac{g_A^2}{Mf_\pi^2} \left\{ I(\omega; k_p, k_p) - I(\omega; k_n, k_n) - K(\omega; k_n, k_p) + \frac{1}{2} [I(0; k_p, k_p) - I(0; k_n, k_n) - K(0; k_n, k_p)] \right\} \\ &+ T^+(\omega) \frac{g_A^2}{Mf_\pi^2} \left\{ I(\omega; k_n, k_n) + I(\omega; k_p, k_p) - I(\omega; k_n, k_p) \right\}. \end{aligned} \quad (18)$$

where again, the sum indicates all possible arrangements of vertices.

The contributions due to diagrams labeled (cr) have also been calculated and are found to be negligibly small (the analytic expressions can be found in Ref. [14]). We have calculated the contribution due to the diagram (ce) and find that its contribution is also negligible. We, therefore, neglect both in our analysis.

The contribution to the pion self-energy due to the pion-two-nucleon current operator in $\mathcal{L}_{\pi NN}^{(1)}$ reads

$$\Pi_{cd}(\omega) = \frac{g_A c_D \omega}{f_\pi^4 \Lambda_\chi} \left(\frac{k_n^3 + k_p^3}{3\pi^2} \right) \left(\frac{k_p^5 - k_n^5}{10\pi^2 M^2} \right), \quad (19)$$

and it appears at order $k_F^8 \omega$. At this order, other diagrams contribute that we are not including. We retain this diagram only to study the sensitivity to higher-order corrections and the low-energy constant c_D .

The only remaining diagrams of Fig. 1 to discuss are the (gp) diagrams, which include one insertion of leading-order nucleon-nucleon (NN) contact interactions between the pion absorption and emission. Due to the isospin flip at the πN vertex, the set of contributing interactions is restricted to the following:

$$\delta\mathcal{L} = g'_1(\bar{n}n)(\bar{p}p) + g'_2(\bar{n}\vec{\sigma}n) \cdot (\bar{p}\vec{\sigma}p) + g'_3(\bar{n}\vec{\sigma}p) \cdot (\bar{n}\vec{\sigma}p). \quad (20)$$

In the past, these short-range interactions, especially in the spin-isospin channel, were important for understanding p-wave condensation, and their repulsive nature ultimately led to the conclusion that p-wave condensation is unlikely. The last low-energy constant g'_3 in Eq.(20) is conventionally written as $g'_3 = g' f^2 / m_\pi^2$ with $f \simeq 1$ and $g' \simeq 0.6$ is the Landau-Migdal parameter [12]. However, when the pion's momentum is zero, all (gp) diagrams vanish in the non-relativistic limit. This contrasts the p-wave case, where (gp) diagrams arise from the pion coupling to nucleon spin-isospin fluctuations at finite momentum.

The pion self-energy at two-loop order is obtained by summing over the individual contributions

$$\Pi_{\text{tot}}(\omega) = \Pi_{ld}(\omega) + \Pi_{ds}(\omega) + \Pi_{ph}(\omega) + \Pi_{pw}(\omega) + \Pi_{cd}(\omega). \quad (21)$$

At the typical densities and isospin asymmetries encountered inside nuclei, the most relevant contributions are due to the terms linear in density and the double-scattering diagram. For example, for $k_n = 280.5$ MeV and $k_p = 243$ MeV, which approximately correspond to the ambient conditions in the central regions of ^{208}Pb , the individual contributions from the diagrams are listed in Table I.

ω	$\Pi_{ld}/2m_\pi$	$\Pi_{ds}/2m_\pi$	$\Pi_{ph}/2m_\pi$	$\Pi_{pw}/2m_\pi$	$\Pi_{cd}/2m_\pi$
m_π	8.8 MeV	7.5 MeV	-0.96 MeV	-0.76 MeV	-0.16 MeV
165 MeV	23.0 MeV	9.5 MeV	-1.14 MeV	-1.3 MeV	-0.18 MeV

TABLE I: Contributions from the individual diagrams to the pion self-energy at $k_n = 280.5$ MeV and $k_p = 243$ MeV using $\tilde{\sigma} = 60$ MeV and $c_D = 1$.

The numerical values in the table are obtained by setting $\tilde{\sigma} = 60$ MeV and $c_D = 1$. Since $\Pi_{ld}(\omega)$ and $\Pi_{ds}(\omega)$ make the dominant contributions, below we shall use pionic atom data to constrain the range for the parameter $\tilde{\sigma}$ defined in Eq. (11).

Experimentally measured energy levels of pionic atoms provide useful constraints on the π^- optical potential in neutron-rich heavy-nuclei such as Pb. In the local density approximation, the optical potential V_s at the center of the pionic atom is related to the local pion-self energy by $V_s = \Pi_{\text{tot}}(\omega - V_C, k_n, k_p)/2\omega$ with $\omega = m_\pi - B$, where B is the binding energy and V_C the Coulomb potential of the nucleus, and k_n, k_p are (local) neutron and proton Fermi momenta, respectively [14].

Phenomenological fits to data suggest that the s-wave component of the π^- optical potential at the center of ^{208}Pb , which we denote as $V_s(^{208}\text{Pb})$, is in the range 28 ± 3 MeV [24, 25]. In Table II we present our results for the optical potential for several values of $\tilde{\sigma}$ obtained using our two-loop calculation of the π^- self-energy.

$\tilde{\sigma}$	40 MeV	50 MeV	60 MeV	70 MeV	80 MeV
$V_s(^{208}\text{Pb})$	24.1 MeV	26.0 MeV	27.9 MeV	29.7 MeV	31.6 MeV

TABLE II: S-wave optical potential at the center of ^{208}Pb . Pionic atoms data indicate that $V_s \simeq 28 \pm 3$ MeV [25].

These values are obtained by assuming that at the center of ^{208}Pb , the baryon density $n_B = 0.16 \text{ fm}^{-3}$, and the proton density $n_p = 0.063 \text{ fm}^{-3}$. We also assumed that $B \simeq 7$ MeV for the ^1S state, and $V_C \simeq -29$ MeV. From Table II we can conclude that experimental constraints on the π^- optical potential require $\tilde{\sigma}$ to be in the range $45 - 75$ MeV. We note that if one assumes that $\tilde{\sigma} \approx \sigma_N$, a recent analysis of pion-nucleon scattering data that favor $\sigma_N \simeq 60$ MeV [26] is contained in our range for $\tilde{\sigma}$.

III. MODELING NN INTERACTIONS

The calculation of the pion self-energy presented in the preceding section neglected interactions between nucleons and assumed that the energies of the nucleons were unaffected by the medium. However, the energy difference between neutrons and protons can be quite large in dense matter. It is important to include this energy difference in calculating the pion self-energy, in particular, because it alters energy denominators associated with diagrams that include intermediate neutron-proton particle-hole states. A consistent approach to include this effect would be based on Chiral Effective Field Theory (χ EFT) [17], as it systematically accounts for short-range interactions and interactions mediated by pions. However, the predictive power χ EFT for $n_B \gtrsim 2n_{\text{sat}}$ is not well understood because truncation errors can grow rapidly at these densities (see Ref. [27] for a recent review). Instead, we adopt a phenomenological model to perform a parametric study of the pion self-energy in dense matter.

The model we adopt is based on a mean-field description of nuclear interactions. It is characterized by just two key parameters: the nuclear symmetry energy and the effective mass of the nucleons. In general, the strength of phenomenological, short-range interactions in mean field models is chosen to reproduce nuclear masses and bulk properties of matter such as its energy density, pressure, and susceptibilities. A common feature of mean-field models is the modification of the single-particle nucleon energies due to their coupling to the mean field generated by other nucleons in the medium. In a large class of these models, the neutron and proton energies are given by

$$E_n(p) = \frac{p^2}{2M_n^*} + \Sigma_n, \quad E_p(p) = \frac{p^2}{2M_p^*} + \Sigma_p. \quad (22)$$

Here, $\Sigma_{n,p}$ are the mean-field energy shifts, and $M_{n,p}^*$ are the effective masses of neutrons and protons in the medium. The mean field energy shift and the effective masses depend on the baryon density and the isospin asymmetry. For simplicity, we neglect the difference between neutron and proton effective masses and assume that $M_n^* = M_p^* = M^*$.

Using nucleon propagators that include mean field energy shifts and a common nucleon effective mass M^* , we have calculated the pion self-energy discussed in the previous section. We find these modifications only affect those diagrams that contain both neutron and proton intermediate states. In particular, the diagrams in Fig. 1 labeled (ph), (pw), and (cd) are the only ones changed, and the modification is to multiply the corresponding expressions in Eqs. (15), (18), and (19) by the factor

$$\xi(\omega) = \frac{\omega}{\omega - (\Sigma_n - \Sigma_p)}, \quad (23)$$

and to make the substitution $M \rightarrow M^*$. In our parametric study, the density dependence of the nucleon effective mass is given by

$$M^* = M \left(1 - \alpha \frac{n_B}{n_{\text{sat}}} \right), \quad (24)$$

and we vary the parameter α in the range $0 \dots 0.1$ to explore the range predicted by microscopic calculations [28, 29]. The factor $\xi(\omega)$ can resonantly enhance the contribution from these diagrams when $\omega \simeq \Sigma_n - \Sigma_p$. Interestingly, in beta-equilibrated neutron star matter, the enhancement factor $\xi(\omega)$ can be simplified by reexpressing the energy difference $\Sigma_n - \Sigma_p$ in terms of the nuclear symmetry energy and the nucleon effective mass. This is accomplished by first noting that the isospin chemical potential $\hat{\mu}$, and the proton, neutron, and electron chemical potentials are related through

$$\hat{\mu} = \mu_e = \mu_n - \mu_p, \quad (25)$$

and that furthermore $\mu_e = 4S(n_B)(1 - 2x)$, where $S(n_B)$ is the nuclear symmetry energy and x the proton fraction. Substituting these relations into $\xi(\omega)$ yields

$$\xi(\omega) = \frac{\omega}{\omega - 4S(n_B)(1 - 2x) + (k_n^2 - k_p^2)/2M^*}, \quad (26)$$

where $k_n = (3\pi^2 n_B(1 - x))^{1/3}$ and $k_p = (3\pi^2 n_B x)^{1/3}$ are the neutron and proton Fermi momenta. As stated previously, $\xi(\omega)$, when large, can change the importance of Feynman diagrams. To estimate this, note that if a pion is produced in the medium, then its frequency is forced to $\omega = \mu_e$. Making this substitution into $\xi(\omega)$ one finds that the diagram labelled (ph), which originally contributed at $\mathcal{O}(k_F^5 \mu_e)$ now contributes at $\mathcal{O}(k_F^3 \mu_e^2)$; the diagram labelled (pw), which originally contributed at $\mathcal{O}(k_F^6 \mu_e)$ now contributes at $\mathcal{O}(k_F^4 \mu_e^2)$; and the diagram labelled (cd), which

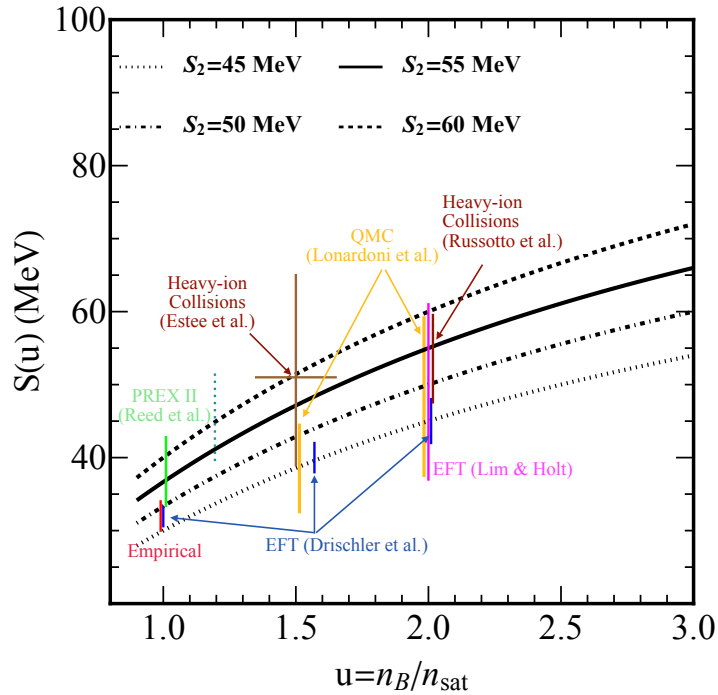


FIG. 2: Experimental and theoretical constraints on the density dependence of the nuclear symmetry energy. Predictions of the parametrization in Eq.31 are shown for reference.

originally contributed at $\mathcal{O}(k_F^8 \mu_e)$ now contributes at $\mathcal{O}(k_F^6 \mu_e^2)$. Crucially, in neutron-rich matter these enhanced diagrams are attractive for positive frequencies.

Through its appearance in the enhancement factor $\xi(\omega)$, the nuclear symmetry energy $S(n_B)$ plays a central role in our calculation. The nuclear symmetry energy is defined through the difference

$$S(n_B) = E(n_B, x = 0) - E(n_B, x = 1/2), \quad (27)$$

where $E(n_B, x)$ is the energy per baryon at baryon density n_B and proton fraction x . Microscopic calculations and fits to phenomenological models indicate that the energy per particle at arbitrary proton fraction is well approximated by

$$E(n_B, x) \approx E(n_B, x = 1/2) + S(n_B)(1 - 2x), \quad (28)$$

since higher order terms in the expansion have been found to be small, even for $x \ll 1/2$ [30]. In this case, the electron chemical potential in neutron star matter is

$$\mu_e(n_B) = 4S(n_B)(1 - 2x). \quad (29)$$

Recently, there has been much interest in determining the density dependence of the symmetry energy. However, despite progress in both theory and experiment, this dependence remains poorly known at densities reached in neutron stars. In the vicinity of nuclear saturation density, $S(n_B)$ impacts nuclear structure. Nuclear masses, measurements of the neutron-skin thickness, and the electric-dipole polarizability of neutron-rich nuclei such as ^{208}Pb provide useful constraints on $S_0 = S(n_{\text{sat}})$. Its density dependence is characterized by the slope parameter $L = 3n_B (dS(n_B)/dn_B)$ at $n_B = n_{\text{sat}}$ [31]. Until recently, experiments, when combined with theoretical models, suggested the empirical range $S_0 = 32 \pm 2$ MeV and $L = 50 \pm 15$ MeV. Theoretical calculations using nucleon-nucleon interactions determined by χ EFT predict S_0 and L compatible with this empirical range. For example, a recent calculation that combines many-body perturbation theory (MBPT) and Bayesian estimates for the truncation errors predicts $S_0 = 31.7 \pm 1.1$ MeV and $L = 59.8 \pm 4.1$ MeV [32]. However, the recent measurement of the neutron-skin thickness of ^{208}Pb using parity-violating electron scattering imply larger values: $S_0 = 38.1 \pm 4.7$ MeV, and $L = 106 \pm 37$ MeV [33, 34].

The symmetry energy at higher density can be accessed in heavy-ion experiments but is not presently well-determined [35]. At $n_B \simeq 1.5 n_{\text{sat}}$, a recent analysis by Estee et al. of charged pion yields from intermediate-energy

heavy-ion collisions suggests that $S(n_B \simeq 1.5n_{\text{sat}}) = 52 \pm 13$ MeV [36]. Earlier studies by Russotto et al. of heavy-ion collisions at GSI indicate that $S(n_B \approx 2n_{\text{sat}}) = 50 \pm 7$ MeV [37].

Theoretical calculations of the equation of state using potentials derived from χ EFT also provide useful constraints on the symmetry energy in the region $n_{\text{sat}} < n_B < 2n_{\text{sat}}$. Quantum Monte Carlo calculations by Lonardoni et al., using local χ EFT potentials predict $S(1.5n_{\text{sat}}) \approx 37 \pm 5$ MeV and $S(2n_{\text{sat}}) \approx 46 \pm 11$ MeV [38]. In Ref. [39], Lim and Holt use many-body perturbation theory (MBPT) to predict $S(2n_{\text{sat}}) \approx 49 \pm 12$ MeV, and Drischler et al., combine MBPT and Bayesian estimates of the χ EFT truncation errors (but neglect errors associated with low energy constants) to predict $S(2n_{\text{sat}}) \approx 45 \pm 3$ MeV [32]. These constraints are shown in Fig. 2.

The density dependence of the symmetry energy is typically written as an expansion about $n_B = n_{\text{sat}}$:

$$S(n_B) = S_0 + L \left(\frac{u-1}{3} \right) + \frac{K_{\text{sym}}}{2!} \left(\frac{u-1}{3} \right)^2 + \frac{Q_{\text{sym}}}{3!} \left(\frac{u-1}{3} \right)^3, \quad (30)$$

where $u = n_B/n_{\text{sat}}$, and the parameters S_0 , L , K_{sym} , and Q_{sym} are chosen to ensure compatibility with experimental constraints. However, because the parameters K_{sym} and Q_{sym} are poorly constrained, the predictions of Eq. (30) at $n_B \gtrsim 2n_{\text{sat}}$ vary over a wide range. In this study, we adopt a simple ansatz for the density dependence of the symmetry energy

$$\tilde{S}(n_B) = \frac{2S_2 u}{2+u}, \quad (31)$$

which depends on a single parameter $S_2 = S(2n_{\text{sat}})$, the symmetry energy at twice saturation density. From Fig. 2 it is clear that S_2 in the range 45 – 60 MeV satisfies all existing constraints. The high value $S_2 = 60$ MeV is compatible with the large S_0 and L predicted by PREX and is implied by the heavy-ion data, and the intermediate value $S_2 \simeq 50$ MeV is compatible with the empirical range. The low value $S_2 = 45$ MeV is in reasonable agreement with the χ EFT predictions made in Ref. [32].

IV. RESULTS & DISCUSSION

In this section, we gather our results. We begin by examining the behavior of the inverse propagator as a function of frequency. A typical plot of the inverse propagator at baryon density $n_B = 2n_{\text{sat}}$ is shown in Fig. 3. Here we have taken the following “typical” values of the scattering parameters: $\tilde{\sigma} = 60$ MeV, $\gamma = 2.6$, $\Lambda_\chi = 700$ MeV, $c_D = 2.6$. We have also taken $S_2 = 50$ MeV, and $\alpha = 0.07$ in our mean-field description of nucleon-nucleon interactions, which lie roughly in the middle of the acceptable range. The plot shows that interactions significantly alter the self-energy compared to the free theory (shown by the dashed curve), which produces a parabolic dispersion with zeros at $\pm m_\pi$.

The poles of the propagator, or the zeros of the inverse propagator, correspond to real excitations in the medium. The energy and charge associated with these excitations are determined by examining the residue at the pole. When the mean field splitting of the neutron and proton energies is neglected (blue curve), the propagator has two poles, as expected in the vacuum. The pole at positive frequency has a positive residue, as can be inferred from examining the slope of the inverse propagator, and is denoted by ω_+ . Since we are examining the two-point function of a *negatively* charged field, this implies that the charge associated with the pole at ω_+ is negative and its effective mass $m_{\pi^-}^* = \omega_+$. The pole at negative frequency denoted by ω_- has a negative residue. It thereby corresponds to the π^+ state with effective mass $m_{\pi^+}^* = -\omega_-$. At this density, $m_{\pi^-}^* \simeq 400$ MeV, and this significant increase is largely due to the energy-dependent Weinberg-Tomozawa term that results in a strong and repulsive s-wave interaction at leading order. In contrast, the reduction of the π^+ effective mass is modest. This is also largely due to the energy-dependent Weinberg-Tomozawa term. The contributions of the individual Feynman diagrams depicted in Fig. 1 to the pion self-energy are shown in the right panel. In the vicinity of the poles corresponding to the π^\pm modes, beyond-leading-order contributions to the self-energy are modest, and there are large cancellations between various two-loop contributions. When mean-field effects are included, the poles of the propagator are shifted. Both π^+ and π^- effective masses are reduced. However, the reduction is modest because, as mentioned earlier, they are both dominated by the leading order contribution, which is insensitive to the mean-field energies. Another noteworthy feature of the result shown in the left panel of Fig. 3 is that the inverse propagator is small (compared with m_π^2) over a fairly wide interval in ω around $\omega = 0$.

A striking feature of mean field effects is that it predicts a third pole corresponding to a collective excitation with a positive charge but negative energy. This collective state has the quantum numbers of the positively charged pion and arises as a coherent proton-particle-neutron-hole excitation. We denoted this mode by the symbol π_s^+ to be consistent with the notation used in earlier work to describe a similar mode at finite momentum [7]. We note that the negative energy of the π_s^+ does not imply instability. The large electron chemical potential ensures that energy associated with

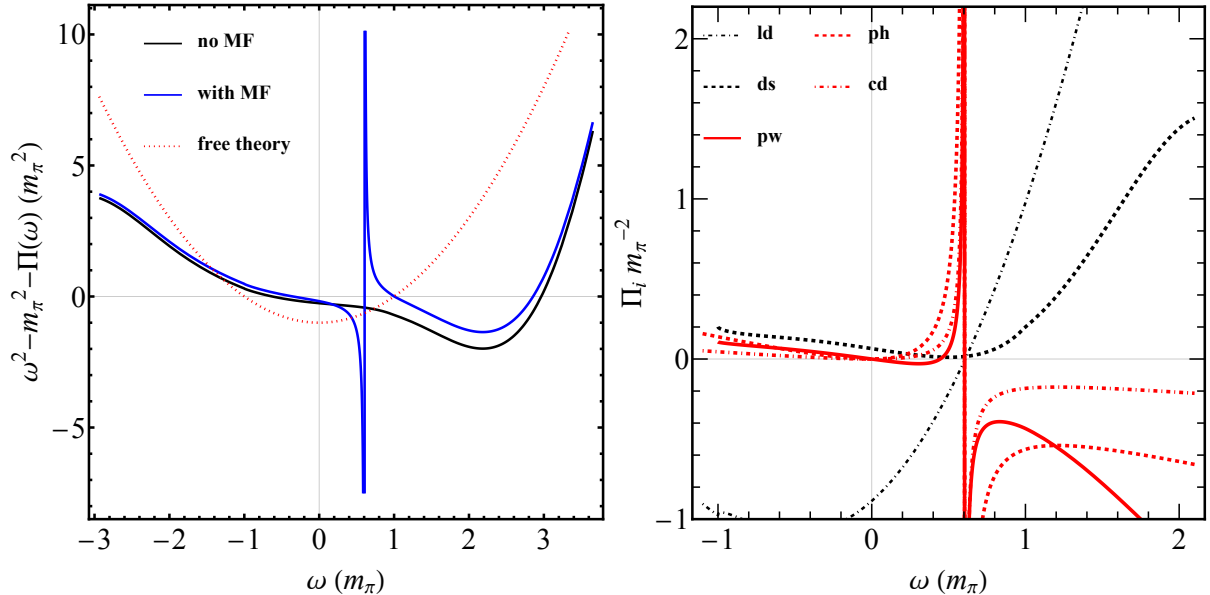


FIG. 3: Left panel: Inverse propagator at two loops with and without mean field corrections as a function of frequency. Here, $n_B = 2n_{\text{sat}}$ and the interaction parameters $\tilde{\sigma} = 60$ MeV, $\gamma = 2.6$, $\Lambda_\chi = 700$ MeV, $c_D = 2.6$, $S_2 = 50$ MeV, $\alpha = 0.07$. Right panel: Individual contribution from the diagrams depicted in Fig. 1 to the pion self-energy.

producing π_s^+ through the reactions $p \rightarrow n\pi_s^+$, given by $\delta\omega_s = \mu_n - \mu_p + \omega_{\pi_s^+} = \omega_{\pi_s^+} + \mu_e$ is positive. The ground state is generally unstable when $\delta\omega_i = m_i^* - \mu_i < 0$, where μ_i is the chemical potential associated with the conserved charge labeled i , and m_i^* is the effective mass of the particle in the ground state. In charge neutral neutron-rich matter in beta-equilibrium, the electric charge chemical potential $\mu_Q = -\mu_e$, where $\mu_e = \mu_n - \mu_p > 0$. From the right panel of Fig. 3 we can infer that in the vicinity of the pole associated with the π_s^+ , the two-loop contribution to the pion self-energy is not much suppressed compared to the leading-order term.

The density dependence of the in-medium masses of the charged pions are shown in Fig. 4. The leading order s-wave WT contribution to the self-energy dominates the π^- mode for the full range of densities considered. Its rapid increase with increasing density precludes s-wave condensation of negatively charged pions. In contrast, the mass of the π^+ mode decreases with density. In this case, the s-wave WT interaction dominates at low density. Higher-order contributions become important for $n_B > n_{\text{sat}}$ resulting in a rapid decrease of the π^+ mass at higher density. As discussed earlier, the mass of the collective mode labeled π_s^+ is negative and decreases with density. Its value is sensitive to the mean-field energy shifts of the nucleons and the two-loop contributions to the pion self-energy. For the density range considered here, $\delta\omega_\pm > 0$ and $\delta\omega_s > 0$. Thus the normal ground state without pion condensation is stable, and the energy to create a $\pi^- - \pi_s^+$ pair is also positive.

V. CONCLUSIONS

We have constructed a model for the pion self-energy in neutron star matter which accounts for important aspects of the pion-nucleon interaction discounted in earlier investigations. The model consists of a two-loop calculation of the pion self-energy within heavy-baryon chiral perturbation theory, which is augmented by in-medium modifications to the nucleon propagators. These modifications include energy shifts and effective masses of the nucleons due to interactions with the nuclear medium. Qualitative changes arise from these modifications. In particular, small energy denominators are produced, which modify the power counting of Feynman diagrams. Certain attractive two-loop diagrams (in this paper denoted $\Pi_{ph}(\omega)$, $\Pi_{pw}(\omega)$, $\Pi_{cd}(\omega)$) are enhanced, especially at energies comparable to the energy splitting between neutrons and protons.

Our parametric study of the self-energy has revealed general trends which we describe in the following. The pion self-energy at zero momentum is found to be strongly energy dependent and the dressed pion propagator has a complex structure with three poles. Two of these poles coincide with the charged pion modes in vacuum in the limit of vanishing density. The third pole corresponds to a new collective excitation that contains an admixture of nucleon particle-hole states with quantum numbers of a positively charged pion. At the poles corresponding to the charged pions modes, the one-loop leading-order (in the density expansion) s-wave diagram remains the dominant

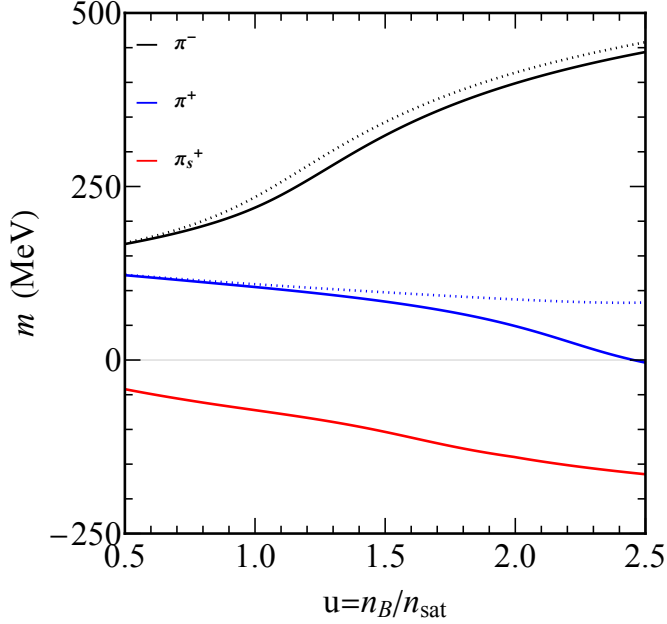


FIG. 4: Masses of the charged pions and the pion-like collective excitation in neutron-rich matter (model parameters used are described in the text). The leading-order (in the density expansion) results are shown by dashed-curves, and the solid curves show the two-loop calculation.

contribution. This is especially true for the π^- where the repulsive s-wave interaction greatly increases the in-medium mass and precludes s-wave pion condensation even for the case of a large symmetry energy. The in-medium mass of the π^+ is reduced due to the attractive s-wave interaction. At high density, the two-loop contribution becomes relevant and accelerates its decrease with increasing density. Our prediction of a positively charged collective mode in the long-wavelength limit is new. The energy of this mode is negative, and its value is sensitive to the energy splitting of neutrons and protons in the medium, the one-loop particle-hole diagram, and the two-loop diagram that involves a p-wave interaction between pions and nucleons.

The phenomenological implications of the low-energy collective mode and the large splitting between the masses of the charged pion excitations warrant further study. We speculate that the collective mode can play a role in neutrino interactions, and the strongly modified and energy-dependent pion propagator can alter nuclear interactions at large distances.

ACKNOWLEDGEMENTS

The work of S. R. and N. C. W. was supported by the U.S. DOE under Grant No. DE-FG02- 00ER41132. B. F. acknowledges support from the SciDAC Grant No. A18-0354-S002 (de-sc0018232). We thank Paulo Bedaque, Gordon Baym, Evgeny Epelbaum, David Kaplan, Thomas Schafer, Achim Schwenk, and Corbinian Wellenhofer for helpful conversations. We also thank Avraham Gal and Eli Friedman for useful correspondence relating to pionic atoms. The work of S. R. was performed in part while attending the "Exploring Extreme Matter in the Era of Multimessenger Astronomy: from the Cosmos to Quarks" workshop at the Aspen Center for Physics.

- [1] R. F. Sawyer, Phys. Rev. Lett. **29**, 382 (1972).
- [2] D. J. Scalapino, Phys. Rev. Lett. **29**, 386 (1972).
- [3] R. F. Sawyer and D. J. Scalapino, Phys. Rev. D **7**, 953 (1973).
- [4] A. Migdal, Physics Letters B **45**, 448 (1973).
- [5] G. Baym, Phys. Rev. Lett. **30**, 1340 (1973).
- [6] G. Baym and E. Flowers, Nucl. Phys. A **222**, 29 (1974).

[7] N. Chi-Kwan Au and G. Baym, Nucl. Phys. A **236**, 500 (1974).

[8] R. F. Dashen and J. Manassah, Phys. Lett. B **50**, 460 (1974).

[9] S. Barshay and G. Brown, Phys. Lett. B **47**, 107 (1973).

[10] W. Weise and G. Brown, Physics Letters B **58**, 300 (1975).

[11] S.-O. Backman and W. Weise, Physics Letters B **55**, 1 (1975).

[12] T. E. O. Ericson and W. Weise, *Pions and Nuclei* (Clarendon Press, Oxford, UK, 1988).

[13] B. Fore and S. Reddy, Phys. Rev. C **101**, 035809 (2020).

[14] E. E. Kolomeitsev, N. Kaiser, and W. Weise, Phys. Rev. Lett. **90**, 092501 (2003), arXiv:nucl-th/0207090.

[15] N. Kaiser and W. Weise, Phys. Lett. B **512**, 283 (2001), arXiv:nucl-th/0102062.

[16] N. Fettes, U.-G. Meißner, and S. Steininger, Nucl. Phys. A **640**, 199 (1998), arXiv:hep-ph/9803266.

[17] E. Epelbaum, H.-W. Hammer, and U.-G. Meißner, Rev. Mod. Phys. **81**, 1773 (2009), arXiv:0811.1338 [nucl-th].

[18] E. Epelbaum, A. Nogga, W. Gloeckle, H. Kamada, U. G. Meißner, and H. Witala, Phys. Rev. C **66**, 064001 (2002), arXiv:nucl-th/0208023.

[19] S. Weinberg, Phys. Rev. Lett. **17**, 616 (1966).

[20] Y. Tomozawa, Nuovo Cim. A **46**, 707 (1966).

[21] M. E. Sainio, PiN Newslett. **16**, 138 (2002), arXiv:hep-ph/0110413.

[22] M. Hoferichter, J. Ruiz de Elvira, B. Kubis, and U.-G. Meißner, Phys. Rev. Lett. **115**, 092301 (2015), arXiv:1506.04142 [hep-ph].

[23] S. Borsanyi, Z. Fodor, C. Hoelbling, L. Lellouch, K. K. Szabo, C. Torrero, and L. Varnhorst, (2020), arXiv:2007.03319 [hep-lat].

[24] E. Friedman and A. Gal, Phys. Lett. B **432**, 235 (1998), arXiv:nucl-th/9805004.

[25] E. Friedman, Phys. Lett. B **524**, 87 (2002), arXiv:nucl-th/0107050.

[26] M. Hoferichter, J. Ruiz de Elvira, B. Kubis, and U.-G. Meißner, Phys. Lett. B **760**, 74 (2016), arXiv:1602.07688 [hep-lat].

[27] C. Drischler, J. W. Holt, and C. Wellenhofer, (2021), 10.1146/annurev-nucl-102419-041903, arXiv:2101.01709 [nucl-th].

[28] X. L. Shang, A. Li, Z. Q. Miao, G. F. Burgio, and H. J. Schulze, Phys. Rev. C **101**, 065801 (2020), arXiv:2001.03859 [nucl-th].

[29] B.-A. Li, B.-J. Cai, L.-W. Chen, and J. Xu, Prog. Part. Nucl. Phys. **99**, 29 (2018), arXiv:1801.01213 [nucl-th].

[30] B.-A. Li, L.-W. Chen, and C. M. Ko, Phys. Rept. **464**, 113 (2008), arXiv:0804.3580 [nucl-th].

[31] A. W. Steiner, M. Prakash, J. M. Lattimer, and P. J. Ellis, Phys. Rept. **411**, 325 (2005), arXiv:nucl-th/0410066 [nucl-th].

[32] C. Drischler, R. J. Furnstahl, J. A. Melendez, and D. R. Phillips, Phys. Rev. Lett. **125**, 202702 (2020), arXiv:2004.07232 [nucl-th].

[33] D. Adhikari *et al.* (PREX), Phys. Rev. Lett. **126**, 172502 (2021), arXiv:2102.10767 [nucl-ex].

[34] B. T. Reed, F. J. Fattoyev, C. J. Horowitz, and J. Piekarewicz, Phys. Rev. Lett. **126**, 172503 (2021), arXiv:2101.03193 [nucl-th].

[35] C. J. Horowitz, E. F. Brown, Y. Kim, W. G. Lynch, R. Michaels, A. Ono, J. Piekarewicz, M. B. Tsang, and H. H. Wolter, J. Phys. G **41**, 093001 (2014), arXiv:1401.5839 [nucl-th].

[36] J. Estee *et al.* (SRIT), Phys. Rev. Lett. **126**, 162701 (2021), arXiv:2103.06861 [nucl-ex].

[37] P. Russotto *et al.*, Phys. Rev. C **94**, 034608 (2016), arXiv:1608.04332 [nucl-ex].

[38] D. Lonardoni, I. Tews, S. Gandolfi, and J. Carlson, Phys. Rev. Res. **2**, 022033 (2020), arXiv:1912.09411 [nucl-th].

[39] Y. Lim and J. W. Holt, Phys. Rev. Lett. **121**, 062701 (2018), arXiv:1803.02803 [nucl-th].

Appendix A: Loop functions

In this appendix, we give analytical expressions for the pertinent functions $I(\omega; k_n, k_p)$, $I(0, k_n, k_n)$, $K(\omega; k_n, k_p)$ and $K(0; k_n, k_p)$ that appear in the contribution $\Pi_{pw}(\omega)$ to the pion selfenergy. In order to evaluate the Fermi sphere integrals in Eq.(17), three nontrivial integrations over the cosine of an inclined angle and two radii have to be performed. The angular integral leads to logarithms and by treating these as logarithms of absolute values the principal-value prescription is effectively implemented. One finds:

$$384\pi^4 I(\omega; k_n, k_p) = \frac{32}{3} k_n^3 k_p^3 + Q^2 L(\omega; k_n, k_p), \quad (\text{A1})$$

with $Q = \sqrt{\omega^2 - m_\pi^2}$ and the function $L(\omega; k_n, k_p)$ is written in Eq.(13). The other loop functions read:

$$384\pi^4 I(0; k_n, k_n) = \frac{32}{3} k_n^6 - 24k_n^4 m_\pi^2 + 4k_n^2 m_\pi^4 + 32k_n^3 m_\pi^3 \arctan \frac{2k_n}{m_\pi} - m_\pi^4 (12k_n^2 + m_\pi^2) \ln \left(1 + \frac{4k_n^2}{m_\pi^2} \right), \quad (\text{A2})$$

$$\begin{aligned} 192\pi^4 K(\omega; k_n, k_p) &= 4k_n k_p (k_n^2 - k_p^2) (k_n^2 + k_p^2 - 5Q^2) + (k_n^2 - k_p^2) \left[(k_n^2 - k_p^2)^2 - 6Q^2 (k_n^2 + k_p^2) - 3Q^4 \right] \\ &\quad \times \ln \frac{|(k_n - k_p)^2 - Q^2|}{|(k_n + k_p)^2 - Q^2|} + 8Q^3 \left[(k_n^3 + k_p^3) \ln \frac{|k_n - k_p - Q|}{|k_n - k_p + Q|} + (k_n^3 - k_p^3) \ln \frac{|k_n + k_p + Q|}{|k_n + k_p - Q|} \right], \quad (\text{A3}) \end{aligned}$$

$$\begin{aligned}
192\pi^4 K(0; k_n, k_p) = & 4k_n k_p (k_n^2 - k_p^2) (k_n^2 + k_p^2 + 5m_\pi^2) + (k_n^2 - k_p^2) \left[3m_\pi^4 - 6m_\pi^2 (k_n^2 + k_p^2) - (k_n^2 - k_p^2)^2 \right] \\
& \times \ln \frac{(k_n + k_p)^2 + m_\pi^2}{(k_n - k_p)^2 + m_\pi^2} + 16m_\pi^3 \left[(k_n^3 + k_p^3) \arctan \frac{k_n - k_p}{m_\pi} + (k_p^3 - k_n^3) \arctan \frac{k_n + k_p}{m_\pi} \right]. \quad (\text{A4})
\end{aligned}$$